electronics

MDPI

Article

LEO-SOP Differential Doppler/INS Tight Integration Method Under Weak Observability

Lelong Zhao [1,2], Ming Lei [1,2], Yue Liu [1,2], Yiwei Wang [1], Jian Ge [1], Xinnian Guo [3] and Zhibo Fang [1,*]

[1] Aerospace Information Research Institute (AIR), Chinese Academy of Sciences, Beijing 100094, China; zhaolelong22@mails.ucas.ac.cn (L.Z.); leiming20@mails.ucas.ac.cn (M.L.); liuyue212@mails.ucas.ac.cn (Y.L.); wangyiwei@aircas.ac.cn (Y.W.); jian.ge@aoe.ac.cn (J.G.)
[2] School of Electronic, Electrical and Communication Engineering, University of Chinese Academy of Sciences, Beijing 100049, China
[3] Suqian Key Laboratory of Visual Inspection and Intelligent Control, Suqian University, Suqian 223800, China; xinnianguo@squ.edu.cn
* Correspondence: fangzb@aircas.ac.cn

Abstract: The utilization of low Earth orbit (LEO) satellites' signals of opportunity (SOPs) for absolute positioning and navigation in global navigation satellite system (GNSS)-denied environments has emerged as a significant area of research. Among various methodologies, tightly integrated Doppler/inertial navigation system (INS) frameworks present a promising solution for achieving real-time LEO-SOP-based positioning in dynamic scenarios. However, existing integration schemes generally overlook the key characteristics of LEO opportunity signals, including the limited number of visible satellites and the random nature of signal broadcasts. These factors exacerbate the weak observability inherent in LEO-SoOP Doppler/INS positioning, resulting in difficulty in obtaining reliable solutions and degraded positioning accuracy. To address these issues, this paper proposes a novel LEO-SOP Doppler/INS tight integration method that incorporates trending information to alleviate the problem of weak observability. The method leverages a parallel filtering structure combining extended Kalman filter (EKF) and Rauch–Tung–Striebel (RTS) smoothing, extracting trend information from the quasi-real-time high-precision RTS filtering results to optimize the EKF positioning solution for the current epoch. This approach effectively avoids the overfitting problem commonly associated with directly using batch data to estimate the current epoch state. The experimental results validate the improved positioning accuracy and robustness of the proposed method.

Keywords: LEO-SOP; doppler; tight integration; RTS; observability

Academic Editor: Felipe Jiménez

Received: 2 December 2024
Revised: 3 January 2025
Accepted: 7 January 2025
Published: 9 January 2025

Citation: Zhao, L.; Lei, M.; Liu, Y.; Wang, Y.; Ge, J.; Guo, X.; Fang, Z. LEO-SOP Differential Doppler/INS Tight Integration Method Under Weak Observability. *Electronics* **2025**, *14*, 250. https://doi.org/10.3390/electronics14020250

1. Introduction

The global navigation satellite system (GNSS) serves as the backbone of the position, navigation, and timing (PNT) system [1–3]. However, its performance is severely compromised in challenging propagation environments such as urban canyons or rural areas with significant shadowing, where positioning errors can escalate to hundreds of meters or even lead to complete service failure [4,5]. Additionally, the weak signal power of the GNSS at the Earth's surface, a consequence of the high orbital altitudes of its satellites, renders it highly vulnerable to interference [6]. This susceptibility becomes particularly evident in environments with strong electromagnetic disturbances, causing difficulties in acquiring and tracking navigation signals. It is necessary to develop alternative or backup navigation schemes for GNSS-denied environments [7,8].

Among various alternatives, the positioning technique based on opportunity signals from low Earth orbit (LEO) non-cooperation and non-navigation satellites is gradually becoming a research focus due to its capability to enable absolute positioning akin to the GNSS [9,10]. Unlike the GNSS, LEO satellites operate at much lower altitudes, resulting in stronger signal power at ground level, superior interference resistance, and better signal penetration [11,12]. The use of Doppler information for positioning is an effective and promising solution in the development of LEO signals of opportunity (SOPs). However, real-time dynamic positioning based solely on Doppler measurements remains challenging. In dynamic scenarios, the instantly visible number of LEO communication satellites is limited, leading to the underdetermination of the Doppler single-point positioning equations. While some studies have achieved real-time positioning using angle-of-arrival (AOA) methods relying solely on LEO-SOPs, these approaches require customized array antennas and precise angle-of-arrival information [13,14]. Continuous dynamic real-time positioning of LEO-SOPs is commonly achieved by tight integration with inertial navigation systems (INS) and other supplementary devices such as barometers [15,16]. However, existing LEO-SOP/INS integration methods fail to adequately account for challenges such as the stochastic nature of LEO signal broadcasts and the limited visibility of satellites. These factors lead to weak system observability, hampering reliable and accurate positioning in such scenarios. It is necessary to develop integration schemes that are appropriate to the characteristics of LEO opportunity signals.

At present, there is no efficient solution to the problems of low observability and nonlinear errors in the LEO-SOP/INS system. Due to the limited number of instantaneously visible satellites and few single epoch Doppler observations of typical LEO constellations such as Orbcomm and Iridium, LEO-SOPs have insufficient constraints on LEO/INS system variables, resulting in weak observability and poor positioning capabilities [17,18]. Conventional differential positioning structures are generally employed to achieve real-time tight integration of single epoch LEO-SOP/INS data [19–21]. However, such methods are significantly dependent on the accuracy of the system parameters, such as the stochastic model. They work effectively in GNSS scenarios with sufficient observation information and well-estimated parameters while struggling to maintain accuracy in the weakly observable environments of LEO-SOP/INS systems, where parameter mismatch and noise discrepancies further degrade performance. Some research has also considered utilizing multi-epoch data to alleviate the weak observability problem, such as the factor graph methods or unbiased finite impulse response (UFIR) methods, which combine historical data to perform instantaneous dynamic positioning [22–24]. However, these methods all rely on the assumption of broad sense stationarity, which means the state error and noise are assumed to follow a Gaussian distribution within a given time window. In reality, the motion of vehicle dynamics scenarios is entirely random, and the state equation has strong nonlinear characteristics, restricting these methods. There are no other practical solutions. Therefore, guaranteeing the LEO-SOP/INS system's real-time performance and handling nonlinear errors while effectively combining multiple history data to achieve improved positioning accuracy and robustness is the primary problem to be solved in this paper.

Existing LEO-SOP/INS tight integration methods also overlook the problems caused by the randomness of LEO signal broadcasting, which involves two main aspects. The first aspect is that the randomness of signal broadcasts causes intermittent disruptions to the LEO-SOP measurements [25,26]. The correction of the system positioning accuracy during the LEO measurement interruption period has not been incorporated into the existing LEO-SOP/INS methods. The second aspect is that the integrated navigation system's restart effect and the subsequent filter convergence are difficult to guarantee when the LEO signal is re-established after a prolonged interruption. Doppler measurements are

too few to provide strong observable navigation information, and the system requires relatively reliable initial values to ensure filter convergence. Typically, additional signal sources such as the GNSS are employed to provide accurate position information to support the convergence of the filters in existing LEO-SOP/INS methods [19,20,27,28]. However, in actual scenarios where the GNSS and other SOP sources are rejected, the limited real-time single-point localization capability of LEO-SOPs may result in unreliable navigation parameter convergence results upon system restart. Therefore, the second motivation of this study is to develop positioning strategies that effectively mitigate the challenges mentioned above in LEO-SOPs positioning scenarios.

In response to the above problems, this paper proposes a tightly integrated navigation method to address the weak observability problem in LEO-SOP/INS positioning. The primary contributions of this paper are as follows:

(1) A novel LEO-SOP/INS method is proposed that alleviates the problem of weak observability by using trend information extracted from batch data. The method is based on a two-channel parallel filter structure in combination with the extended Kalman filter (EKF) and the Rauch–Tung–Striebel (RTS) smoother. The structure combines the trend information extracted from the RTS batch-processing results to optimize the stochastic model of the real-time positioning channel and adjusts the dimension of the navigation parameters.

(2) A complete LEO-SoOP/INS positioning solution is proposed, which addresses supplementary issues such as post-processing bridging of positioning results during measurement loss divergence and system initialization. Based on the designed parallel filtering structure, the solution ensures real-time positioning while achieving high-precision post-processing of the positioning results and bridging of the positioning results during measurement interruptions.

(3) The reasonableness and effectiveness of the proposed method were verified. The proposed method's validity is demonstrated in comparison to the conventional EKF method through both simulation and on-board experiments, and the applicability of the proposed method is thoroughly discussed.

The summary of this paper's organization is as follows: Section 2 illustrates the design and principles of the proposed method. Section 3 presents the simulation and in-vehicle experiments conducted to illustrate the effectiveness of the proposed method. Section 4 conducts a practical analysis of the method. Section 5 summarizes this paper's contributions, innovations, and future research directions.

2. Methodology

In this section, a differential Doppler/INS tight integration method is proposed to address the challenges of weak observability in LEO-SOP positioning scenarios. The overall framework and underlying principles of the method are first introduced. Subsequently, the design and workflow of the EKF-RTS parallel filter structure are detailed, including the collaborative mechanism between the real-time filtering module and the quasi-real-time high-precision filtering module. At the same time, this paper points out the optimization approach of the stochastic model and the adjustment strategy of the navigation parameter dimensions within the parallel filter structure.

2.1. Overall Framework of the Proposed Method

The overall structure of the method is shown in Figure 1. The EKF-RTS parallel filter structure is the main component of the method, consisting of two output channels: a real-time response channel and a quasi-real-time high-precision channel. The EKF channel ensures tight integration with the real-time response. Trend information is extracted from

the high-precision post-processing results of the quasi-real-time channel to serve the real-time EKF channel. Specifically, the trend information utilization method incorporates stochastic model correction and navigation parameter dimension adjustment to improve positioning accuracy and robustness.

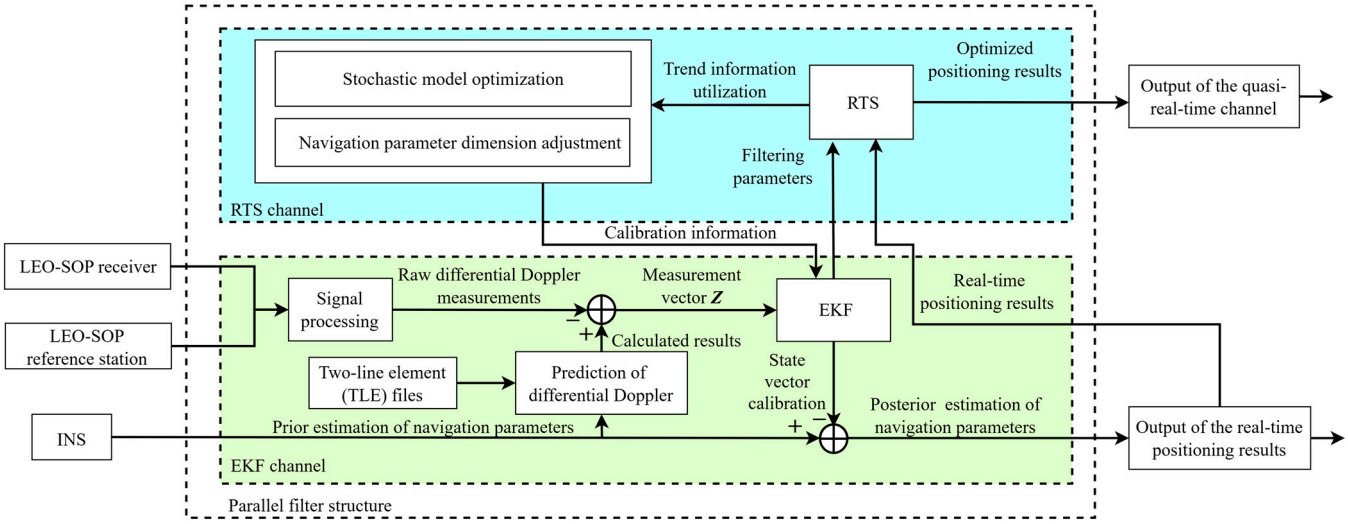

Figure 1. Overall logical structure of the proposed method.

2.2. Differential Doppler Measurement Model and System State Model

The state vector and Doppler measurement model of the LEO-SOP/INS tight integration method are initially introduced. The positions of LEO satellites derived from the LTE ephemeris may contain orbital errors up to several kilometers, causing significant errors in the Doppler measurements [29]. Considering the short baseline scenario [30], this paper employs the single-station differential approach to improve positioning accuracy and reduce the impacts of satellite orbit errors, ionospheric errors, and tropospheric errors. The state vector of the tightly integrated differential system in a short baseline dynamic scenario is defined as follows:

$$\begin{cases} \boldsymbol{X}_k = \begin{bmatrix} \delta \boldsymbol{p}^T & \delta \boldsymbol{v}^{nT} & \delta \boldsymbol{\phi}^T & \boldsymbol{\varepsilon}^T & \nabla^T \end{bmatrix}^T \\ \delta \dot{\boldsymbol{p}} = \delta \boldsymbol{v}^n + \boldsymbol{\omega}_{en}^n \times \delta \boldsymbol{p} \\ \delta \dot{\boldsymbol{v}}^n = \boldsymbol{f}^n \times \boldsymbol{\phi} + \boldsymbol{v}^n \times \left(2\delta \boldsymbol{\omega}_{ie}^n + \delta \boldsymbol{\omega}_{en}^n\right) - \left(2\boldsymbol{\omega}_{ie}^n + \boldsymbol{\omega}_{en}^n\right) \times \delta \boldsymbol{v}^n + \delta \boldsymbol{f}^n \\ \delta \dot{\boldsymbol{\phi}} = \delta \boldsymbol{\phi} \times \boldsymbol{\omega}_{in}^n + \delta \boldsymbol{\omega}_{in}^n - \delta \boldsymbol{\omega}_{ib}^n \end{cases} \tag{1}$$

where, $\boldsymbol{X}_k$ is the system state vector at the time step k, $\delta \boldsymbol{p}$ is the position error vector in the navigation coordinate frame (denoted with superscript n), $\delta \boldsymbol{v}^n$ is the velocity error vector in the navigation coordinate frame, $\delta \boldsymbol{\phi}$ is the attitude error vector in the carrier coordinate frame, $\boldsymbol{\varepsilon}$ is the accelerometer bias error vector, ∇ is the gyroscope bias error vector, $\delta \dot{\boldsymbol{p}}$, $\delta \dot{\boldsymbol{v}}^n$, and $\delta \dot{\boldsymbol{\phi}}$ are the corresponding time derivatives of $\delta \boldsymbol{p}$, $\delta \boldsymbol{v}^n$, and $\delta \boldsymbol{\phi}$, respectively, $\boldsymbol{f}^n$ is the specific force of the accelerometer in the navigation coordinate frame, $\delta \boldsymbol{f}^n$ is the error vector of $\boldsymbol{f}^n$, $\boldsymbol{\omega}_{en}^n$ is the angular rate of the earth's rotation in the navigation coordinate frame, $\boldsymbol{\omega}_{ie}^n$ is the angular rate of the gyroscope output, and $\boldsymbol{\omega}_{in}^n$ is the projection of the rotation angle rate of the navigation coordinate frame relative to the inertial coordinate frame in the navigation coordinate frame, and $\boldsymbol{\omega}_{in}^n = \boldsymbol{\omega}_{ie}^n + \boldsymbol{\omega}_{en}^n$. $\delta \boldsymbol{\omega}_{in}^n$, $\delta \boldsymbol{\omega}_{ie}^n$, and $\delta \boldsymbol{\omega}_{en}^n$ are the corresponding corresponding angular rate errors of $\boldsymbol{\omega}_{in}^n$, $\boldsymbol{\omega}_{ie}^n$, and $\boldsymbol{\omega}_{en}^n$, respectively. The update of the system's position, velocity, and attitude error state vectors is performed through the INS model.

The Doppler measurements can be obtained by specialized LEO-SOP receivers [20]. A direct frequency estimation of the LEO signals using fast Fourier transform (FFT) can provide a coarse estimate of the Doppler frequency [11]. Currently, advanced Doppler frequency estimation methods can control the frequency estimation error to around 2 Hz [31], fully meeting the requirements for the proposed method and common high-precision positioning applications [21]. The Doppler measurement models of the reference station and the user receiver are as follows:

$$\begin{cases} \dot{\rho}_u^{(i)} = (\dot{\boldsymbol{x}}_s^{(i)} - \dot{\boldsymbol{x}}_u^{(i)}) \frac{\boldsymbol{x}_s^{(i)} - \boldsymbol{x}_u}{\left\| \boldsymbol{x}_s^{(i)} - \boldsymbol{x}_u \right\|} + c(\dot{\delta} t_u - \dot{\delta} t_s^{(i)}) + \dot{T}_u^{(i)} + \dot{I}_u^{(i)} + \nu_u^{(i)} \\ \dot{\rho}_r^{(i)} = (\dot{\boldsymbol{x}}_s^{(i)})' \frac{\boldsymbol{x}_s^{(i)} - \boldsymbol{x}_r}{\left\| \boldsymbol{x}_s^{(i)} - \boldsymbol{x}_r \right\|} + c(\dot{\delta} t_r - \dot{\delta} t_s^{(i)}) + \dot{T}_r^{(i)} + \dot{I}_r^{(i)} + \nu_r^{(i)} \end{cases} \tag{2}$$

where, $\dot{\rho}_r^{(i)}$ is the Doppler of the i-th LEO satellite measured by the reference station, $\dot{\rho}_u^{(i)}$ is the Doppler of the i-th LEO satellite measured by the user receiver, $\dot{\boldsymbol{x}}_s^{(i)}$ is the three-dimensional position vector of the i-th LEO satellite in the Earth-centered, Earth-fixed (ECEF) coordinate frame, $\boldsymbol{x}_r$ is the position vector of the reference station in the ECEF coordinate frame, $\boldsymbol{x}_u$ is the position vector of the user receiver in the ECEF coordinate frame, $\dot{\boldsymbol{x}}$ is the three-dimensional velocity vector, and the upper and lower subscripts have the same meaning as the position vectors, c is the speed of light, $\dot{\delta} t_s^{(i)}$ is the clock drift of the i-th LEO satellite, $\dot{\delta} t_r$ is the clock drift of the reference station, $\dot{\delta} t_u$ is the clock drift of the user receiver, $\dot{T}_u^{(i)}$ and $\dot{I}_u^{(i)}$ are the tropospheric and ionospheric delay rates of the user receiver, $\dot{T}_r^{(i)}$ and $\dot{I}_r^{(i)}$ are the tropospheric and ionospheric delay rates of the reference station, $\nu_r^{(i)}$ and $\nu_u^{(i)}$ are the Doppler measurement noise of the reference station and user receiver to the i-th satellite, which are modeled as discrete-time zero-mean Gaussian white sequences. $(\dot{\boldsymbol{x}}_s^{(i)} - \dot{\boldsymbol{x}}_u^{(i)}) \frac{\boldsymbol{x}_s^{(i)} - \boldsymbol{x}_u}{\left\| \boldsymbol{x}_s^{(i)} - \boldsymbol{x}_u \right\|}$ and $(\dot{\boldsymbol{x}}_s^{(i)})' \frac{\boldsymbol{x}_s^{(i)} - \boldsymbol{x}_r}{\left\| \boldsymbol{x}_s^{(i)} - \boldsymbol{x}_r \right\|}$ represent the Doppler prediction processes for the receiver and reference station, respectively, with respect to the i-th satellite.

In the short baseline scenarios, it is assumed that the line-of-sight vectors of the reference station and the receiver between the same satellite are parallel [32]. Therefore, the differential equation of the LEO differential Doppler model between the receiver and the reference station is:

$$\delta z_{\dot{\rho}}^{(i)} = \delta \dot{\rho}_r^{(i)} - \delta \dot{\rho}_u^{(i)} = \boldsymbol{s}_r^{(i)} \cdot \delta \boldsymbol{x}_u + \boldsymbol{e}_r^{(i)} \cdot \delta \dot{\boldsymbol{x}}_u + c \dot{\delta} t_{r,u} + \dot{T}_{r,u}^{(i)} + \dot{I}_{r,u}^{(i)} + \nu_{r,u}^{(i)} \tag{3}$$

where

$$\begin{cases} \boldsymbol{e}_r^{(i)} = \frac{\boldsymbol{x}_s^{(i)} - \boldsymbol{x}_r}{\left\| \boldsymbol{x}_s^{(i)} - \boldsymbol{x}_r \right\|} \\ \boldsymbol{s}_r^{(i)} = \frac{\left(\dot{\boldsymbol{x}}_s^{(i)\prime} - \boldsymbol{e}_r^{(i)} \cdot \left(\boldsymbol{e}_r^{(i)} \cdot \dot{\boldsymbol{x}}_s^{(i)\prime} \right) \right)}{\left\| \boldsymbol{x}_s^{(i)} - \boldsymbol{x}_r \right\|} \\ \dot{\delta} t_{r,u} = \dot{\delta} t_r - \dot{\delta} t_u \\ \dot{T}_{r,u}^{(i)} = \dot{T}_r^{(i)} - \dot{T}_u^{(i)} \\ \dot{I}_{r,u}^{(i)} = \dot{I}_r^{(i)} - \dot{I}_u^{(i)} \\ \nu_{r,u}^{(i)} = \nu_r^{(i)} - \nu_u^{(i)} \end{cases} \tag{4}$$

where, $\delta z_{\dot{\rho}}^{(i)}$ is the differential Doppler measurement between the reference station and the receiver of the i-th LEO satellite, $\boldsymbol{e}_r^{(i)}$ is the equivalent line-of-sight unit vector from the receiver to the i-th satellite, $\boldsymbol{s}_r^{(i)}$ is the equivalent relative velocity vector from the receiver to the i-th satellite, $\dot{\delta} t_{r,u}$ is the differential clock drift between the reference station and the receiver, $\dot{T}_{r,u}^{(i)}$ is the differential tropospheric delay rate between the reference station and

the receiver, $\dot{I}_{r,u}^{(i)}$ is the differential ionospheric delay rate between the reference station and the receiver, and $\nu_{r,u}^{(i)}$ is the differential measurement noise between the reference station and the user receiver. Equation (4) presents the calculation process for $\dot{\delta}t_{r,u}$, $\dot{T}_{r,u}^{(i)}$, $\dot{I}_{r,u}^{(i)}$ and $\nu_{r,u}^{(i)}$. In addition, when considering short baseline scenarios, the line-of-sight vectors between the reference station and the mobile station and the line-of-sight vectors between the reference station and the mobile station are assumed to be parallel. Therefore, the equivalent line-of-sight unit vector $\boldsymbol{e}_r^{(i)}$ can be obtained by calculating the line-of-sight unit vector between the reference station and the corresponding satellite, as shown in Equation (4). The equivalent relative velocity vector $\boldsymbol{s}_r^{(i)}$ is also calculated in this way. When considering land-vehicle application scenarios, the velocity of the receiver is ignored for the sake of the calculation of $\boldsymbol{s}_r^{(i)}$. The velocity vector of satellite $\dot{\boldsymbol{x}}_s^{(i)\prime}$ is used here to represent the relative velocity vector between the receiver and the satellite in the calculation process of $\boldsymbol{s}_r^{(i)}$. The explanation is as follows. Taking the Orbcomm satellite speed of 7.5474 km/s as an example, when considering the car vehicle or pedestrian application scenarios, the receiver speed is considerably lower than the satellite speed, making the receiver speed negligible in the calculation of the relative speed between the receiver and the satellite. In addition, LEO-SOP receivers generally adopt high-precision atomic clocks. The clock errors can be accurately calculated and corrected in advance, so the clock errors are not estimated in this paper [33]. At this point, the relationship between the measurement model and the state model is:

$$\boldsymbol{Z} = \left[\delta z_{\dot{\rho}}\right]^T = \boldsymbol{H}\boldsymbol{X}_k \tag{5}$$

where

$$\begin{cases} \boldsymbol{Z} = \left[\delta z_{\dot{\rho}}^{(1)} \quad \delta z_{\dot{\rho}}^{(2)} \quad \cdots \quad \delta z_{\dot{\rho}}^{(n)}\right]^T \\ \boldsymbol{H} = \begin{bmatrix} \boldsymbol{s}_r^{(1)} & \boldsymbol{e}_r^{(1)} & \boldsymbol{0}_{1\times 3} & \boldsymbol{0}_{1\times 3} & \boldsymbol{0}_{1\times 3} \\ \vdots & \vdots & \vdots & \vdots & \vdots \\ \boldsymbol{s}_r^{(n)} & \boldsymbol{e}_r^{(n)} & \boldsymbol{0}_{1\times 3} & \boldsymbol{0}_{1\times 3} & \boldsymbol{0}_{1\times 3} \end{bmatrix} \end{cases} \tag{6}$$

where, $\boldsymbol{Z}$ is the measurement vector, $\boldsymbol{H}$ is the coefficient matrix, and n is the total number of co-viewing satellites.

2.3. Parallel Filter Structure

The combination and utilization of multi-epoch data is a viable way to alleviate the problem of weak observability. However, reasonable batch-processing results must be obtained by post-processing in combination with future data. At the same time, we propose that under the permission of quasi-real-time processing, methods such as post-processing can be considered to integrate into the navigation system to connect interrupted parts. Therefore, this paper proposes a parallel filter structure. It utilizes a two-channel approach to enhance the positioning accuracy and robustness of the localization results. This structure can not only extract information from historical data, taking advantage of multi-epoch data processing to some extent, but also ensure real-time performance and cope with nonlinear errors. Initially, the implementation principle and function of each filter channel in the parallel filter structure are introduced in the EKF-RTS section. Then, the collaboration between the channels and the optimization of the system is introduced in the Stochastic Model and State Vector Dimension Optimization section.

2.3.1. EKF-RTS

The tight integration method works in the pattern of parallel dual-channel output. The real-time channel adopts normal EKF forward filtering, using single-differential Dopplers as the raw measurements, as follows:

$$\boldsymbol{X}_{f,k} = \boldsymbol{\Phi}_{k,k-1}\boldsymbol{X}_{f,k-1} + \boldsymbol{W}_{k-1} \tag{7}$$

$$\boldsymbol{Z}_k = \boldsymbol{H}_k\boldsymbol{X}_{f,k} + \boldsymbol{V}_k \tag{8}$$

where, $\boldsymbol{X}_{f,k}$ is the prior estimation state vector at time step k, $\boldsymbol{\Phi}_{k,k-1}$ is the state-transition matrix, which can be obtained from Equation (1), $\boldsymbol{X}_{f,k-1}$ is the prior estimation vector at time step $k-1$, $\boldsymbol{W}_{k-1}$ is the process noise vector, $\boldsymbol{Z}_k$ is the measurement vector at time step k, $\boldsymbol{H}_k$ is the relationship matrix between the measurement vector and the state vector at time step k, and $\boldsymbol{V}_k$ is the measurement noise vector. Forward filtering uses the EKF to perform in real time to ensure the real-time positioning result output of the positioning scheme.

Considering the update interval difference between the LEO-SOP receiver and the INS sensors, here is a supplementary explanation of the system's positioning solution process. In the epoch where the LEO-SOPs are not obtained, the navigation state increment result of the current and last epoch is calculated based on the inertial sensor. Then, the navigation state increment is added to the navigation state estimation of the last epoch to calculate the positioning result of the current epoch. In epochs where the LEO-SOPs are received, Equation (8) is called to further correct the error increment of the system state. At the same time, with the LEO-SOPs received, the system further invokes the quasi-real-time processing channel to optimize the system state within a certain time window, as described below.

The quasi-real-time channel employs the RTS smoother. The initial value of the RTS smoother is derived from the EKF filter result at the current time. Interval smoothing is performed based on a predetermined interval size to obtain the optimal quasi-real-time smoothing result, as implemented below:

$$\boldsymbol{K}_{s,k} = \boldsymbol{P}_{f,k}\boldsymbol{\Phi}_{k+1,k}^{T}\boldsymbol{P}_{f,k+1|k}^{-1} \tag{9}$$

$$\hat{\boldsymbol{X}}_{s,k} = \hat{\boldsymbol{X}}_{f,k} + \boldsymbol{K}_{s,k}\left(\hat{\boldsymbol{X}}_{s,k+1} - \hat{\boldsymbol{X}}_{f,k+1|k}\right) \tag{10}$$

$$\boldsymbol{P}_{s,k} = \boldsymbol{P}_{f,k} + \boldsymbol{K}_{s,k}\left(\boldsymbol{P}_{s,k+1} - \boldsymbol{P}_{f,k+1|k}\right)\boldsymbol{K}_{s,k}^{T} \tag{11}$$

where, $\boldsymbol{K}_{s,k}$ is the gain matrix of the RTS smoother at time step k, $\boldsymbol{P}_{f,k}$ is the forward filtering posterior covariance matrix at time step k, $\boldsymbol{\Phi}_{k+1,k}$ is the state-transition matrix from time step k to time step $k+1$, $\boldsymbol{P}_{f,k+1|k}$ is the prior covariance matrix of the forward filtering at time step $k+1$, $\hat{\boldsymbol{X}}_{s,k}$ is the RTS posterior estimation vector at time step k, $\hat{\boldsymbol{X}}_{f,k}$ is the posterior estimation state vector of the forward filtering at time step k, $\hat{\boldsymbol{X}}_{f,k+1|k}$ is posterior estimation state vector of the forward filtering at time step $k+1$, $\boldsymbol{P}_{s,k}$ is the RTS posterior estimated covariance matrix at time step k, and $\boldsymbol{P}_{s,k+1}$ is the RTS posterior estimated covariance matrix at time step $k+1$. The parameters $\boldsymbol{P}_{f,k}$, $\boldsymbol{\Phi}_{k+1,k}$, $\boldsymbol{P}_{f,k+1|k}$, $\hat{\boldsymbol{X}}_{f,k}$, and $\hat{\boldsymbol{X}}_{f,k+1|k}$ can be calculated and stored in real time during the forward filtering and do not need recalculations. The quasi-real-time channel utilizes the filtering results of the real-time channel as input. Subsequently, by using the trend information of the smoothing results of the quasi-real-time channel, the system optimizes the stochastic model and the dimension of the state vector of the EKF to improve real-time positioning. The following section will describe the implementation principle of this process.

2.3.2. Stochastic Model and State Vector Dimension Optimization

When the statistical characteristics of Doppler observation noise vary or are unidentified, the information fusion filters may experience degradation or even divergence in performance due to noise mismatch [34]. Significant interfering noise from receivers and ancillary equipment in dynamic environments can exacerbate the situation. This problem

is particularly severe in weak observability LEO-SOPs scenarios, further limiting the use of the limited measurement information of the integrated navigation system. Therefore, an optimization method for the stochastic model and the state vector dimension is developed on the basis of the parallel filter structure, using the trend information of the batch epoch data to reduce the noise mismatch problem.

The first step is to analyze the error characteristics of the differential Doppler measurements. As shown in Equation (2), there are satellite orbit, ionosphere, and troposphere errors in addition to the observation noise error after the single difference. It is necessary to effectively extract the observation noise to estimate the stochastic model. Within a limited time, the satellite orbit position is subject to slow variations due to disturbing forces, and the satellite orbit error changes within a limited range as the primary source of error. Therefore, it is assumed that the single-differential Doppler residual error has a certain degree of correlation over a limited period.

The positioning results obtained from the quasi-real-time RTS processing are employed to calculate the mean residual error over a specified time window as a residual assessment of the satellite orbit error, ionosphere, troposphere, and satellite orbit error. Then, the extent of the observation noise can be calculated as follows:

$$\begin{cases} \boldsymbol{L}_{r,u}^{(i)} = \delta z_{\rho}^{(i)} - c\dot{\delta} t_{r,u} - \dot{T}_{r,u}^{(i)} - \dot{I}_{r,u}^{(i)} - \nu_{r,u}^{(i)} \\ \Delta \boldsymbol{L}_{r,u}^{(i)}(k) = \frac{1}{w} \sum_{j=k-w+1}^{k} \boldsymbol{L}_{r,u}^{(i)}(j) \\ \boldsymbol{\varsigma} = \boldsymbol{L}_{r,u}^{(i)}(k) - \Delta \boldsymbol{L}_{r,u}^{(i)}(k) \\ \boldsymbol{IR} = \left(\frac{\boldsymbol{\varsigma}}{\delta_0}\right)^2 \cdot \boldsymbol{R}_k \end{cases} \tag{12}$$

where, $\boldsymbol{L}_{r,u}^{(i)}$ is the residual of the differential measurement, $(\cdot)$ means the value of the variable at the corresponding time step, $\Delta \boldsymbol{L}_{r,u}^{(i)}(k)$ is the calculated mean value at the time step k, w is the window size, $\boldsymbol{\varsigma}$ indicates the magnitude of the noise level, $\boldsymbol{IR}$ is the optimized stochastic model, δ_0 is the preset measurement noise variance, and $\boldsymbol{R}_k$ is the measurement noise matrix of the EKF. The differential measurement stochastic model of the real-time EKF is adjusted according to the above formula.

At the same time, the state vector dimension is adjusted based on the observability within the time window interval of the quasi-real-time processing result. If the position state observability is lower than the set threshold, the state parameter dimension of the equation is adjusted as follows:

$$\boldsymbol{X}_k = \begin{bmatrix} \delta \boldsymbol{p}^T & \delta \boldsymbol{v}^{nT} & \delta \boldsymbol{\phi}^T \end{bmatrix}^T \tag{13}$$

The corresponding covariance matrix is adjusted simultaneously. When observability improves, the correction of the gyroscope bias and accelerometer bias is resumed.

3. Experiments and Results

Vehicle dynamic scene experiments were conducted to verify the effectiveness of the proposed LEO-SOP/INS method. The positioning effect of the proposed LEO-SOP/INS method and the normal EKF method was tested by simulation and on-board experiments. The advantages and effectiveness of the proposed method were evaluated in terms of mean deviation, standard deviation (STD), root mean square error (RMSE), and other aspects.

3.1. Simulation Experiment

3.1.1. Experiment Setting

The simulation experiment considers the scenario where both the reference station and the receiver are equipped with high-precision atomic clocks. The clock difference between the reference station and the receiver was corrected in advance. The height direction of the positioning was constrained by a barometer. The parameters of the simulated INS in the simulation experiments are detailed in Table 1. A simulated LEO-SOP receiver was designed specifically to process signals from the Iridium and ORBCOMM constellations for Doppler estimation. For the Iridium constellation, the LEO-SOP receiver estimates the Doppler shifts by leveraging the single-carrier pilot signals embedded in the downlink burst frames transmitted by the Iridium satellites. For the ORBCOMM constellation, Doppler estimation is performed using the symmetrical differential phase-shift keying (SDPSK)-modulated signals within its downlink transmissions. The update interval of the inertial navigation system was 0.01 s, and the update interval for the Doppler results output by the LEO-SOP receiver was 0.1 s. The evolution of the number of visible satellites over time during the experiment is shown in Figure 2. It can be seen that the number of visible satellites never satisfied the instantaneous Doppler single-point positioning calculation during the test. The observability of the LEO-SOP/INS system was weak. During the simulation experiment, the non-holonomic constraint (NHC) assistance was added to the positioning calculation process of both methods to improve the positioning effect.

Table 1. Main parameters of the adopted inertial navigation system in the simulation experiments.

IMU	Gyro Bias (deg/h)	Accelerometer Bias (mg)	Angle Random Walk (deg/h$^{1/2}$)
	0.5	1.250	0.012

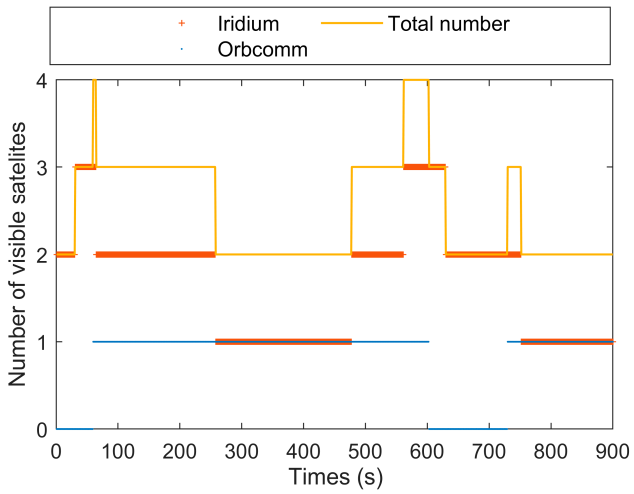

Figure 2. Number of visible satellites during the simulation experiment.

3.1.2. Experiment Results

In the following, the positioning results of the proposed method and the normal method will be compared and analyzed in the local East-North-Up (ENU) coordinate system. Figure 3 compares the positioning results of the two methods in horizontal directions. The positioning results of the proposed method are significantly superior to the normal method. The positioning results of the proposed method are closer to the ground truth and can effectively reflect the vehicle movement trajectory. However, the positioning results

of the normal method show a trend of gradual divergence, and its ability to maintain positioning is less effective than the proposed method.

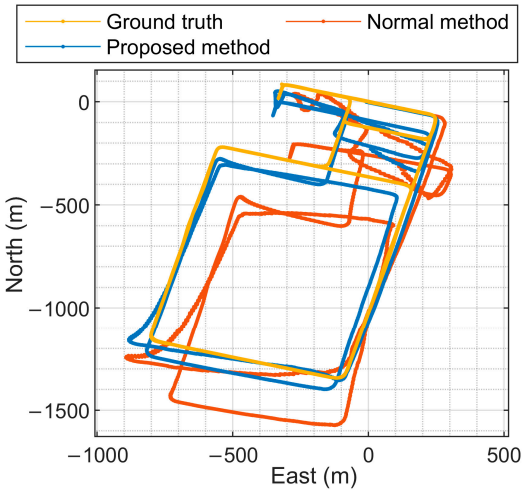

Figure 3. Comparison of positioning results of the two methods in the simulation experiment.

Figure 4 shows the variation in the positioning errors over time in each direction of the two methods. In the horizontal directions, the error levels of the proposed method are generally lower than the normal method, and the errors diverge more slowly than the normal method. Sometimes, the proposed method has difficulty adapting to sudden changes in the scene, i.e., the phenomenon of overfitting occurs, leading to a slight decrease in the positioning effect. This is because the proposed method uses quasi-real-time processing channel information to solve the current positioning problem. Nevertheless, as seen in Figure 4, there are only rare situations where the positioning errors of the proposed method are larger than the normal method. The phenomenon is less likely to occur, and the proposed method can adjust quickly to return to normal error levels after it happens. In addition, the main orbit of the Iridium satellites is north–south, which provides a better constraint on a receiver's position error in the north direction. Therefore, the positioning errors of the two methods are smaller in the north direction than in the east direction. The error levels of the two methods in the up direction are similar. The range of receiver movement in the test was in the order of thousands of kilometers, and the barometer can provide an effective constraint. Due to the barometer's constraints, the upward errors of the two methods do not diverge over time.

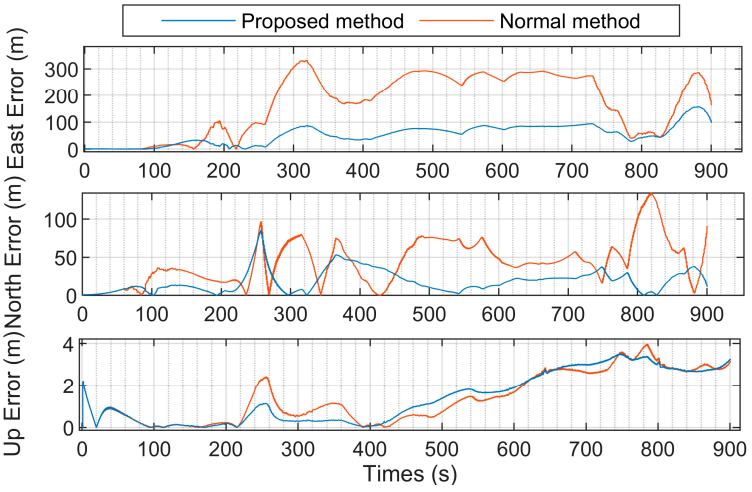

Figure 4. Positioning deviations of the two methods in the simulation experiment.

Figures 5 and 6 show the velocity and attitude estimation results of each method over time, respectively. The velocity parameter estimation results of the proposed method are superior to the normal method in all directions. In combination with the analysis of the position results, the proposed method can effectively estimate the position vector and velocity vector of the receiver in dynamic scenes. As shown in Figure 6, the attitude estimation results of the proposed method are also superior to those of the normal method in all directions.

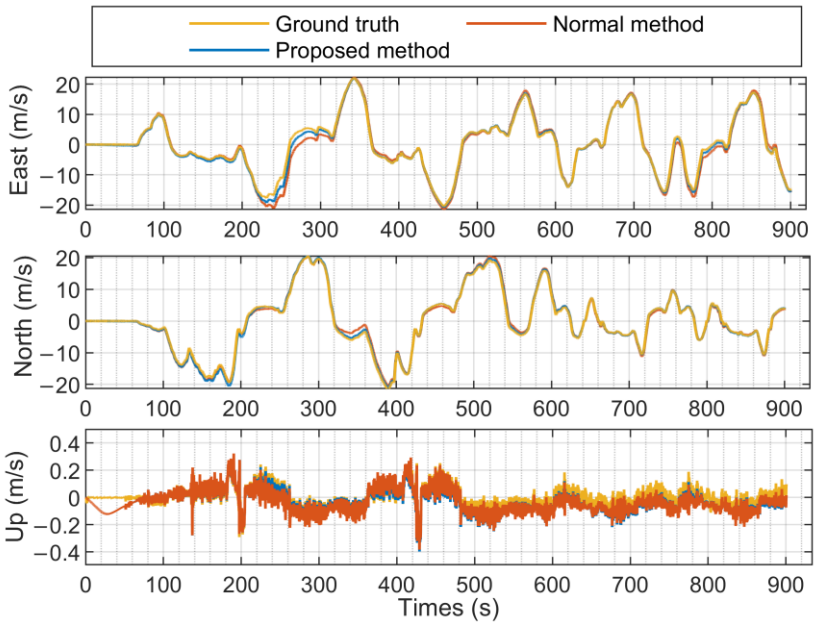

Figure 5. Comparison of the estimated velocity results in the simulation experiment.

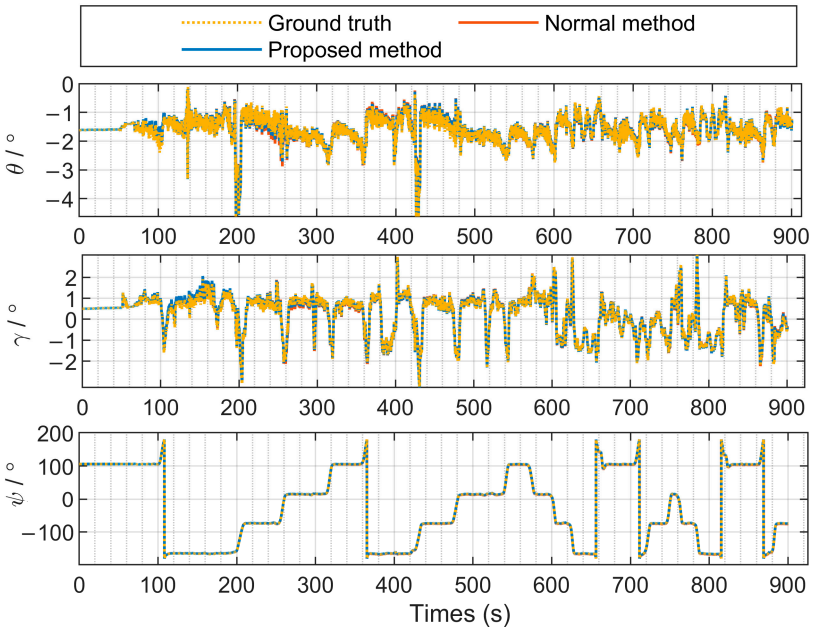

Figure 6. Comparison of the attitude estimation results in the simulation experiment.

Table 2 shows the statistical results of the horizontal directions of the proposed method and the normal method. Compared with the normal method, the improvement effect of the proposed method in terms of the mean deviation, STD, and RMSE has reached more than 45%, demonstrating the effectiveness of the proposed method.

Table 2. Data statistics of positioning results of the two methods in the simulation experiment.

Method and Promotion	Direction	Mean Deviation	STD	RMSE
Proposed method	E	−53.16 m	36.90 m	64.71 m
	N	−16.41 m	17.17 m	23.75 m
Normal method	E	−161.95 m	121.92 m	202.71 m
	N	32.74 m	40.08 m	51.75 m
Promotion	E	67.17%	69.73%	68.07%
	N	49.87%	57.16%	54.10%

3.2. On-Board Experiment

To ensure the practical applicability of the proposed method, further on-board experiments were carried out in typical dynamic vehicle scenarios. The experiment scenario was an open road scene. The positioning results of an RTK/INS high-precision tight coupling integrated navigation system were used as the reference trajectory. During the test, the update interval of the inertial navigation system was 0.01 s, and the update interval for the Doppler results output by the LEO-SOP receiver was 0.1 s. The main parameters of the custom-designed INS sensor employed in this study are shown in Table 3. The LEO-SOP receiver used in the experiments is a custom-built signal receiver developed by our research team. It utilizes the YZNQ9000 series FPGA as the core for signal processing, complemented by a custom low-noise amplifier and specialized antennas for receiving Iridium and Starlink signals. The customized Iridium antenna is designed primarily for receiving single-carrier pilot signals from Iridium's downlink burst frames, which are used for Doppler estimation. The customized Starlink antenna is specifically designed to capture single-carrier signals within fixed bandwidths at 11.325 GHz, 11.575 GHz, and 12.45 GHz for Doppler estimation. The sampling rate of the LEO-SOP receiver for signals from different constellations is uniformly set to 12.5 MHz. The type of baseline between the reference and the receiver was the short baseline. In the on-board experiment, the specific model of the land vehicle employed was the Buick GL8. Sensors such as the LEO-SOP receiver, INS, and GNSS/INS reference were rigidly fixed to the Buick GL8 vehicle.

Table 3. Main parameters of the adopted inertial navigation system in the on-board experiment.

IMU	Gyro Bias (deg/h)	Accelerometer Bias (mg)	Angle Random Walk (deg/$h^{1/2}$)
	1.8	1.5	0.09

The satellite distribution sky map and the variation in the number of visible satellites over time during the test are shown in Figure 7. The time when the instantaneous number of visible satellites is zero accounts for 10.96% of the test time; the time when the instantaneous number of visible satellites is one accounts for 71.6% of the test time; and the time when the number of visible satellites is two accounts for 17.44% of the test time. During the test, the proposed method and the normal method were used for positioning. Both methods employed the data from the same wheel speed sensor and barometer to assist. Moreover, NHC assistance was also added to the positioning calculation process of both methods to improve the positioning effect.

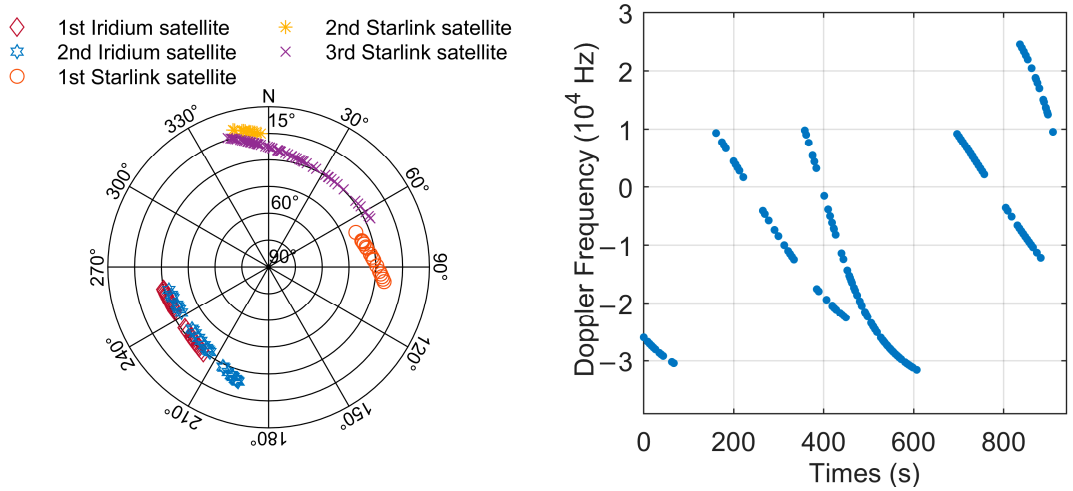

(**a**) (**b**)

Figure 7. Visible satellites and Doppler measurement information during the on-board experiment: (**a**) Satellite distribution sky map during the experiment; (**b**) raw Doppler measurements during the experiment.

Figure 8 shows the positioning results of the proposed method and the normal method. The proposed method's positioning results are closer to the ground truth than the normal method, and its trajectory is smoother. It is clear that the positioning results of the proposed method are significantly superior to the normal method. During the dynamic test, there were short periods when the vehicle was stationary while waiting for the traffic lights. For example, in Figure 9, the position in each direction remains unchanged from 235–420 s to 718–822 s in the position variation curve diagram. This short period of immobility can help the tightly integrated system to converge the positioning errors, as shown by the convergence of the positioning results at the coordinates (−1000 m, −400 m) in Figure 8, indicated by the red frame. It can be seen that the positioning error convergence effect of the proposed method is also better than that of the normal method in all directions. In addition, the positioning errors in the north direction of the two methods are larger than those in the east direction. This is because the main direction of the vehicle movement is east–west, and the wheel speed sensor has a better effect in constraining errors in the main direction of the vehicle movement. Meanwhile, as the orbits of the observed Iridium satellites are north–south, the positioning error in the north direction of the proposed method has been significantly improved compared to the normal method after improving the use of Doppler measurements.

Figure 10 shows the variation in the positioning deviations in each direction over time for the two methods. The up-direction positioning errors of the two methods are well suppressed due to the assistance of the same barometer, and the error levels are similar. The errors in the east and north directions of the proposed method are generally more minor than those of the normal method. It is worth noting that there are times when the positioning errors of the proposed method are more significant than those of the normal method. This is because the sensitivity of the positioning effect of the proposed method is slightly affected, resulting in a slight increase in the positioning errors. However, as shown in Figure 10, the errors can be re-converged and suppressed quickly after the errors increase.

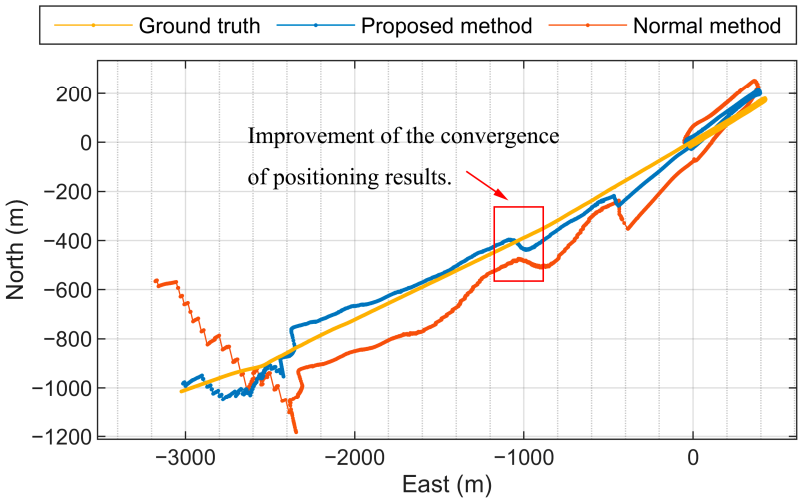

Figure 8. Comparison of positioning results of the two methods in the on-board experiment.

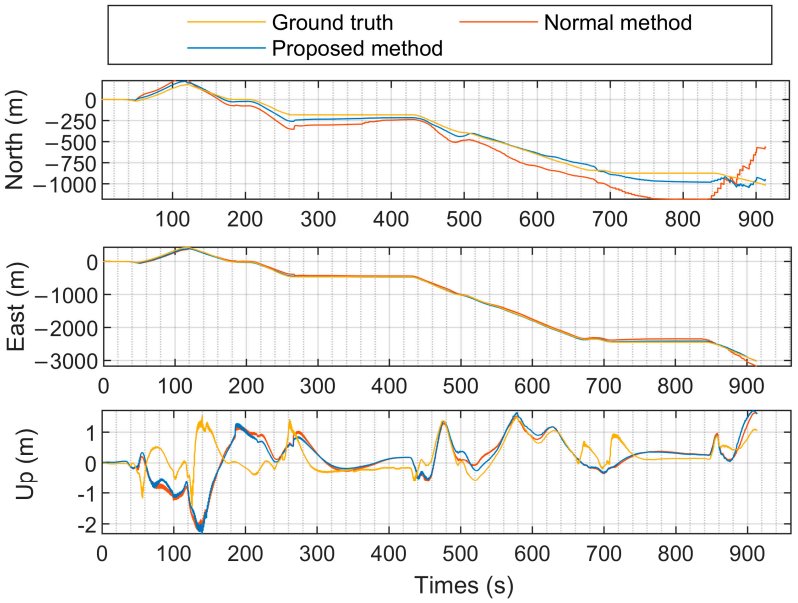

Figure 9. Variation in the positioning results over time in all directions.

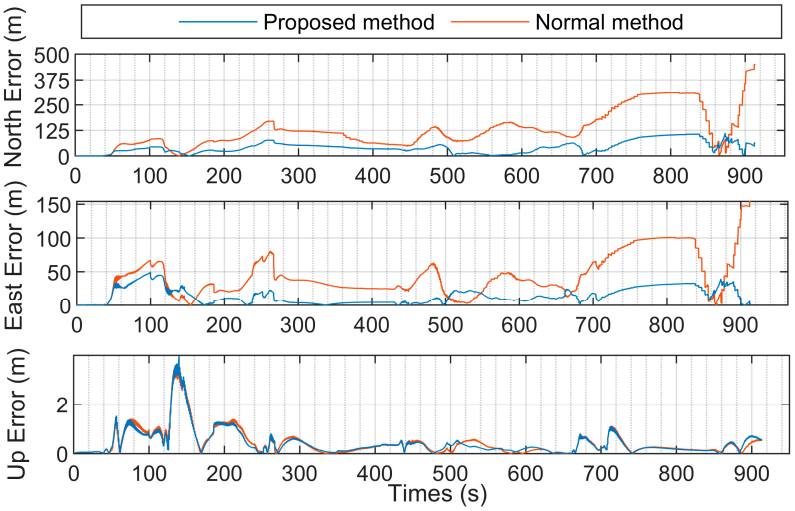

Figure 10. Positioning deviations of the two methods in the on-board experiment.

Table 4 presents the comparison of the positioning performance of the two methods in horizontal directions. Similar to the simulation experiment, the positioning performance improvement in the proposed method over the normal method is more than 45% in the on-board experiment. The addition of the wheel speed sensor constraint in the on-board experiment resulted in better positioning indicators compared to the simulation experiment results in the previous section.

Table 4. Data statistics of positioning results of the two methods in the on-board experiment.

Method & Promotion	Direction	Mean Deviation	STD	RMSE
Proposed method	E	−0.43 m	18.72 m	18.72 m
	N	−23.72 m	43.68 m	45.70 m
Normal method	E	25.50 m	46.27 m	52.85 m
	N	−93.12 m	124.22 m	155.24 m
Promotion	E	98.31%	59.54%	65.00%
	N	74.50%	64.69%	70.53%

Comparative analysis from both simulation and on-board experiments using the INS systems with varying accuracies indicates that when integrated with LEO-SOP measurements, the differences in INS accuracy do not lead to significant changes in the order of magnitude of the final positioning results. Meanwhile, the results demonstrate that in scenarios where LEO-SOP measurements are available, the LEO-SOP effectively mitigates the cumulative divergence of the INS errors. The integrated system can maintain convergence in the positioning results without error divergence over extended navigation periods.

In conclusion, this paper compares the positioning performance of the proposed method and the normal method through multiple simulation experiments and on-board experiments. Based on the above analysis of the positioning results, the novel LEO-SOP/INS tight integration scheme proposed in this paper can achieve an improved positioning effect. Its positioning accuracy and robustness are both superior to the normal system by over 45%, which demonstrates the practical significance of the proposed method.

4. Discussion

Both simulation experiments and on-board experiments were carried out to demonstrate the practicality of the proposed method. In the settings of the two experiments, the accuracy of the inertial navigation system adopted in the simulation experiment is superior to that of the on-board experiment. The on-board experiment utilized the common accuracy inertial navigation system to match the actual application scenario. However, the on-board experiment ultimately achieved better positioning results than the simulation experiment by introducing additional assistance from the wheel speed sensor. In addition, the proposed method has a similar boost on the numerical performance of the positioning results compared to the normal method in the two experiments, both higher than 45%.

Additionally, precise pre-calibration of the INS errors and stochastic drift can enhance the positioning performance of the proposed method. Future research could explore incorporating real-time online calibration of the INS errors to further improve the system's reliability. In the land-vehicle scenarios, the Doppler frequency estimation accuracy provided by existing LEO opportunity signal receivers meets the requirements of this method. Furthermore, the LEO-SOP/INS tightly coupled method ensures the preservation of overall positioning accuracy in dynamic scenarios such as turning or orientation. Future research could explore the development of deeply coupled methods to enhance Doppler frequency accuracy and positioning performance for extreme scenarios such as ultra-high-speed conditions.

In the following, the applicability of the proposed method is analyzed. The main purpose of the proposed method is to address the difficulty of weak observability in low Earth orbit satellite opportunity signal-positioning scenarios. Since the real-time filter channel ensures the output of real-time positioning results, the real-time performance of the proposed method is not affected by the adoption of the parallel filter structure. The proposed method partially uses high-precision post-processed trend information to assist the current epoch positioning. It avoids the overfitting problem caused by directly using raw historical measurements to participate in current epoch positioning. The parallel filter structure also solves the problem of post-correction and connection of the positioning results during measurement interruption periods. To demonstrate the superiority of the method, the experiments in this paper mainly focus on the positioning results in the vehicle scenarios. The application of this method is not limited to the experimental scenario in this paper. The proposed method is also applicable to static, pedestrian, ship-borne, and other related application scenarios. For unmanned aerial vehicle (UAV) application scenarios, the accuracy of attitude estimation could be further enhanced by optimizing the attitude estimation algorithm or employing higher-precision INS devices. These refinements would optimize and improve the method's performance, ensuring its effectiveness in UAV applications.

5. Conclusions

This paper proposes a novel tightly coupled LEO-SOP/INS integration method to address the weak observability issues inherent in LEO opportunity signal-positioning scenarios. Firstly, the method introduces a novel EKF-RTS parallel filtering structure. The structure leverages the trend information of the quasi-real-time high-precision post-processing positioning results to refine the system's stochastic model, thereby enhancing the real-time positioning accuracy and improving robustness to noise adaptation. This structure innovatively extracts trend information from batch data to serve the positioning of the current epoch, avoiding the overfitting phenomenon of directly using batch data for state estimation. Secondly, this paper presents a comprehensive positioning framework based on the forward-backward filtering idea. This framework ensures real-time positioning while simultaneously addressing challenges such as bridging positioning gaps during signal interruptions and achieving high-precision post-processing of the positioning results. Finally, simulations and real-world car-based experiments were conducted, demonstrating that the proposed method improves positioning accuracy by over 45% compared to conventional EKF methods. Furthermore, this method can be extended to other scenarios characterized by weak observability.

Author Contributions: Conceptualization, L.Z. and Z.F.; methodology, L.Z. and M.L.; software, Y.L.; validation, L.Z. and Y.W.; data curation, J.G.; writing—original draft preparation, L.Z.; writing—review and editing, Z.F. and X.G.; supervision, Z.F. All authors have read and agreed to the published version of the manuscript.

Funding: This research was funded by the Strategic Priority Research Program of the Chinese Academy of Sciences, grant number XDA0350403; National Natural Science Foundation of China, grant number 62001183; and the Suqian Sci&Tech Program, grant number M202305.

Data Availability Statement: Data are contained within this article.

Acknowledgments: We are grateful to everyone for their constructive suggestions for improving this manuscript.

Conflicts of Interest: The authors declare no conflicts of interest.

References

1. Thomas, J.; Axel, K.; Rafael, B.; Maarten, W. A Survey on IoT Positioning Leveraging LPWAN, GNSS, and LEO-PNT. *IEEE Internet Things J.* **2023**, *10*, 11135–11159. [CrossRef]
2. Yang, L.; Li, Y.; Wu, Y. An enhanced MEMS-INS/GNSS integrated system with fault detection and exclusion capability for land vehicle navigation in urban areas. *GPS Solut.* **2014**, *18*, 593–603. [CrossRef]
3. Gao, Y.; Li, G. A new asynchronous traction signal spoofing algorithm for PLL-assisted DLL receiver. *GPS Solut.* **2023**, *27*, 141. [CrossRef]
4. Meng, Y.; Weng, D.; Yang, C.; Wu, C.; Hou, Z. Chip-scale atomic clock (CSAC) aided GNSS in urban canyons. *GPS Solut.* **2024**, *28*, 195. [CrossRef]
5. Sun, K.; Yu, B.; Xu, L.; Elhajj, M.; Yotto, W. A Novel GNSS Anti-Interference Method Using Fractional Fourier Transform and Notch Filtering. *IEEE Trans. Instrum. Meas.* **2024**, *73*, 8507617. [CrossRef]
6. Alluhaybi, A.; Psimoulis, P.; Remenyte-Prescott, R. An Evaluation of Optimization Algorithms for the Optimal Selection of GNSS Satellite Subsets. *Remote Sens.* **2024**, *16*, 1794. [CrossRef]
7. Zhang, X.; Huang, Y.; Tian, Y.; Lin, M.; An, J. Noise-Like Features-Assisted GNSS Spoofing Detection Based on Convolutional Autoencoder. *IEEE Sens. J.* **2023**, *23*, 25473–25486. [CrossRef]
8. Crosara, L.; Ardizzon, F.; Tomasin, S.; Laurenti, N. Worst-Case Spoofing Attack and Robust Countermeasure in Satellite Navigation Systems. *IEEE Trans. Inf. Forensics Secur.* **2024**, *19*, 2039–2050. [CrossRef]
9. Khalife, J.; Kassas, Z. Receiver Design for Doppler Positioning with Leo Satellites. In Proceedings of the 2019 IEEE International Conference on Acoustics, Speech and Signal Processing (ICASSP), Brighton, UK, 12–17 May 2019; pp. 5506–5510. [CrossRef]
10. Ries, L.; Limon, M.; Grec, F.; Anghileri, M.; Prieto-Cerdeira, R.; Abel, F.; Miguez, J.; Perello-Gisbert, J.; d'Addio, S.; Ioannidis, R.; et al. LEO-PNT for Augmenting Europe's Space-based PNT Capabilities. In Proceedings of the 2023 IEEE/ION Position, Location and Navigation Symposium (PLANS), Monterey, CA, USA, 24–27 April 2023; pp. 329–337. [CrossRef]
11. Shi, C.; Zhang, Y.; Li, Z. Revisiting Doppler positioning performance with LEO satellites. *GPS Solut.* **2023**, *27*, 126. [CrossRef]
12. Psiaki, M. Navigation using carrier Doppler shift from a LEO constellation: TRANSIT on steroids. *Navig. J. Inst. Navig.* **2021**, *68*, 621–641. [CrossRef]
13. Florio, A.; Bnilam, N.; Talarico, C.; Crosta, P.; Avitabile, G.; Coviello, G. LEO-Based Coarse Positioning Through Angle-of-Arrival Estimation of Signals of Opportunity. *IEEE Access* **2024**, *12*, 17446–17459. [CrossRef]
14. Ellis, P.; Rheeden, D.; Dowla, F. Use of Doppler and Doppler Rate for RF Geolocation Using a Single LEO Satellite. *IEEE Access* **2020**, *8*, 12907–12920. [CrossRef]
15. Yang, Y.; Mao, Y.; Ren, X. Demand and key technology for a LEO constellation as augmentation of satellite navigation systems. *Satell. Navig.* **2024**, *5*, 11. [CrossRef]
16. McLemore, B.; Psiaki, M. Navigation Using Doppler Shift From LEO Constellations and INS Data. *IEEE Trans Aerosp Electron Syst.* **2022**, *58*, 4295–4314. [CrossRef]
17. Morales, J.; Khalife, J.; Kassas, Z. Simultaneous Tracking of Orbcomm LEO Satellites and Inertial Navigation System Aiding Using Doppler Measurements. In Proceedings of the 2019 IEEE 89th Vehicular Technology Conference (VTC2019-Spring), Kuala Lumpur, Malaysia, 28 April–1 May 2019; pp. 1–6. [CrossRef]
18. Kassas, Z.; Kozhaya, S.; Kanj, H.; Saroufim, J.; Hayek, S.; Neinavaie, M.; Khairallah, N.; Khalife, J. Navigation with Multi-Constellation LEO Satellite Signals of Opportunity: Starlink, OneWeb, Orbcomm, and Iridium. In Proceedings of the 2023 IEEE/ION Position, Location and Navigation Symposium (PLANS), Monterey, CA, USA, 24–27 April 2023; pp. 338–343. [CrossRef]
19. Saroufim, J.; Hayek, S.; Kassas, Z. Simultaneous LEO Satellite Tracking and Differential LEO-Aided IMU Navigation. In Proceedings of the 2023 IEEE/ION Position, Location and Navigation Symposium (PLANS), Monterey, CA, USA, 24–27 April 2023; pp. 179–188. [CrossRef]
20. Du, Y.; Qin, H.; Zhao, C. LEO Satellites/INS Integrated Positioning Framework Considering Orbit Errors Based on FKF. *IEEE Trans. Instrum. Meas.* **2024**, *73*, 5501714. [CrossRef]
21. Zhao, C.; Qin, H.; Wu, N.; Wang, D. Analysis of Baseline Impact on Differential Doppler Positioning and Performance Improvement Method for LEO Opportunistic Navigation. *IEEE Trans. Instrum. Meas.* **2023**, *72*, 1–10. [CrossRef]
22. Xu, Y.; Shmaliy, Y.; Bi, S.; Chen, X.; Zhuang, Y. Extended Kalman/UFIR Filters for UWB-Based Indoor Robot Localization Under Time-Varying Colored Measurement Noise. *IEEE Internet Things J.* **2023**, *10*, 15632–15641. [CrossRef]
23. Yuan, D.; Qin, Y.; Wu, Z.; Shen, X. An Emergency Positioning System Fusing GEO Satellite Doppler Observation and INS for SOTM. *IEEE Trans. Instrum. Meas.* **2021**, *70*, 8503804. [CrossRef]
24. Huang, Y.; Zhang, Y.; Zhao, Y.; Shi, P.; Chambers, J. A Novel Outlier-Robust Kalman Filtering Framework Based on Statistical Similarity Measure. *IEEE Trans. Automat. Contr.* **2021**, *66*, 2677–2692. [CrossRef]
25. Tan, Z.; Qin, H.; Cong, L.; Zhao, C. Positioning Using IRIDIUM Satellite Signals of Opportunity in Weak Signal Environment. *Electronics* **2020**, *9*, 37. [CrossRef]

26. Cheng, S.; Cheng, J.; Zang, N. Adaptive non-holonomic constraint aiding Multi-GNSS PPP/INS tightly coupled navigation in the urban environment. *GPS Solut.* **2023**, *27*, 152. [CrossRef]
27. Morales, J.J.; Khalife, J.; Cruz, U.S.; Kassas, Z.M. Orbit Modeling for Simultaneous Tracking and Navigation using LEO Satellite Signals. In Proceedings of the 32nd International Technical Meeting of the Satellite Division of the Institute of Navigation, Miami, FL, USA, 16–20 September 2019.
28. Zhang, S.; Tu, R.; Gao, Z.; Zhang, P.; Wang, S.; Lu, X. Low-Earth-Orbit Satellites and Robust Theory-Augmented GPS/Inertial-Navigation-System Tight Integration for Vehicle-Borne Positioning. *Electronics* **2024**, *13*, 508. [CrossRef]
29. Yang, C.; Zang, B.; Gu, B.; Zhang, L.; Dai, C.; Long, L.; Zhang, Z.; Ding, L.; Ji, H. Doppler Positioning of Dynamic Targets with Unknown LEO Satellite Signals. *Electronics* **2023**, *12*, 2392. [CrossRef]
30. Wu, N.; Qin, H.; Zhao, C. Long-Baseline Differential Doppler Positioning Using Space-Based SOPs Based on BPVGMM. *IEEE Trans. Instrum. Meas.* **2023**, *72*, 8503610. [CrossRef]
31. Yang, M.; Wang, Y.; Fang, Z.; Chen, J.; Liu, Y.; Lei, M.; Xu, Y. A Novel Doppler Estimation Approach Using ORBCOMM Signals for High-Precision Positioning. *Electronics* **2024**, *13*, 4882. [CrossRef]
32. Li, Y.; Zou, X.; Liu, P.; Luo, B.; Pan, W.; Yan, L. Four-Element Array for GNSS Attitude Determination Using IRLS: An Improved Rounding of Long-Short Baseline Approach. *IEEE Trans. Veh. Technol.* **2020**, *69*, 4920–4934. [CrossRef]
33. Manandhar, S.; Saravanan, S.; Meng, Y.S.; Tan, Y.C. A Linear Regression-Based Methodology to Improve the Stability of a Low-Cost GPS Receiver Using the Precision Timing Signals from an Atomic Clock. *Electronics* **2024**, *13*, 3321. [CrossRef]
34. Wu, Q.; Yang, R.; Liu, K.; Xu, Y.; Miao, J.; Sun, M. Dual Kalman Filter Based on a Single Direction under Colored Measurement Noise for INS-Based Integrated Human Localization. *Electronics* **2024**, *13*, 3027. [CrossRef]